ELSEVIER

International Journal of Mass Spectrometry 194 (2000) 181–196

International Journal of Mass Spectrometry

Rearrangement and fragmentation pathways of $[C_3H_7Z]^+$ ions (Z = NH and S): are ion–neutral complexes important?

Andrew J. Chalk[a], Paul M. Mayer[b], Leo Radom[a,*]

[a]*Research School of Chemistry, Australian National University, Canberra ACT 0200, Australia*
[b]*Chemistry Department, University of Ottawa, Ottawa K1N 6N5, Canada*

Received 19 April 1999; accepted 21 April 1999

Abstract

High level ab initio calculations at the G2(ZPE = MP2) level have been used to characterize the potential energy surfaces for rearrangement/fragmentation of various $[C_3H_8N]^+$ and $[C_3H_7S]^+$ isomers. In contrast to the behavior in the corresponding $[C_3H_7O]^+$ system, it is found that ion–neutral complexes are only of minor importance in determining the fragmentation characteristics. Either dissociation of such complexes occurs too fast due to a large barrier to their formation ($[C_3H_8N]^+$ system), or alternative lower-energy rearrangement routes that do not involve ion–neutral complexes are available ($[C_3H_7S]^+$ system). Calculated thermochemical quantities such as heats of formation and reaction barriers are found to be in reasonable agreement with experimental results. Metastable ion product abundances and results of both deuterium- and ^{13}C-labeling experiments are rationalized in terms of the calculated potential energy surfaces and rate constants obtained using Rice-Ramsperger-Kassel-Marcus theory. (Int J Mass Spectrom 194 (2000) 181–196) © 2000 Elsevier Science B.V.

Keywords: $[C_3H_8N]^+$; $[C_3H_7S]^+$; Metastable ion; G2; RRKM; Ion–neutral complex; Heat of formation

1. Introduction

In 1978, Bowen and Williams proposed that elimination of water from the $[CH_3CH_2OCH_2]^+$ metastable ion occurs via a mechanism involving ion–neutral complexes as intermediates [1]. Since that time, numerous examples of the intermediacy of ion–neutral complexes have been discussed [2] and explicit support for their involvement in the rearrangement/fragmentation of $[CH_3CH_2OCH_2]^+$ has come from high-level ab initio studies [3]. Interestingly, experiments on the isoelectronic ions $[CH_3CH_2NHCH_2]^+$ and $[CH_3CH_2SCH_2]^+$ have found that their behavior is quite different from that of the corresponding $[CH_3CH_2OCH_2]^+$ ion [4,5]. In particular, these experiments suggest that ion–neutral complexes may be less important in the decomposition of the former pair of ions [4b,4c,4f,5].

Experimental studies of the metastable decomposition of the $[CH_3CH_2NHCH_2]^+$ ion have found that, in contrast to the behavior of $[CH_3CH_2OCH_2]^+$, only ethylene loss is observed, with exclusive occurrence of β-hydrogen transfer to nitrogen. On the other hand, $[CH_3CH_2SCH_2]^+$ is found to behave more similarly to $[CH_3CH_2OCH_2]^+$, in that both hydrogen sulfide and ethylene are lost during metastable decomposi-

* Corresponding author. E-mail: radom@rsc.anu.edu.au

Dedicated to Professor Jim Morrison on the occasion of his 75th birthday.

PII S1387-3806(99)00127-X

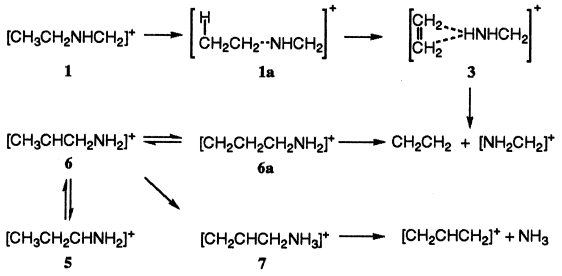

Scheme 1. Originally proposed mechanism [4c] for rearrangement and fragmentation of $[C_3H_8N]^+$ ions

tion. However, again in contrast to the situation for $[CH_3CH_2OCH_2]^+$, the mechanism proposed to explain this observation does not involve the participation of any ion–neutral complexes [5].

Relevant experimental studies of the fragmentation of other metastable $[C_3H_8N]^+$ and $[C_3H_7S]^+$ ions, including several labeling studies, have also been performed [4,5], and detailed mechanisms have been proposed to explain the results of the various experiments (Schemes 1 and 2) [4c,5]. There have also been theoretical investigations on aspects of the potential energy surface for the decomposition of several of the $[C_3H_8N]^+$ isomers [4a,6]. We are not aware, however, of any relevant theoretical studies reported to date on the $[C_3H_7S]^+$ system.

The present work aims to characterize the potential energy surfaces for rearrangement/fragmentation of several $[C_3H_8N]^+$ and $[C_3H_7S]^+$ isomers. Along with Rice-Ramsperger-Kassel-Marcus (RRKM) calculations, these results are used to rationalize the experimentally observed product abundances and labeling patterns, as well as to make comparisons with experimental thermochemical information. The potential surfaces for the systems examined here and our previous theoretical work on $[C_3H_7O]^+$ ions [3b] allow us to identify some of the key factors that determine the importance of ion–neutral complexes in the rearrangement/fragmentation processes.

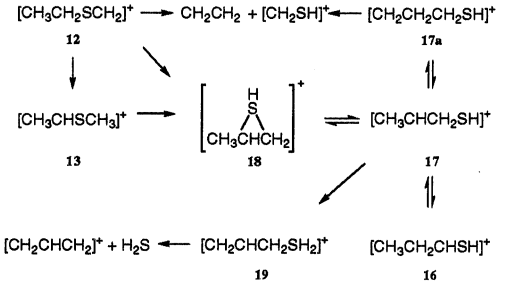

Scheme 2. Originally proposed mechanism [5] for rearrangement and fragmentation of $[C_3H_7S]^+$ ions

2. Methods and results

Standard ab initio molecular orbital calculations [7] have been performed with the GAUSSIAN 94 [8] and MOLPRO96 [9] programs using a modification of the G2 method [10]. The G2 procedure has been shown generally to predict thermochemical quantities to so-called chemical accuracy (± 10 kJ mol^{-1}) [11]. It uses a combination of Hartree-Fock (HF), second-order Møller-Plesset perturbation theory (MP2), and quadratic configuration interaction with single, double, and perturbative triple excitations (QCISD(T)) procedures and corresponds effectively to QCISD(T)/6-311+G(3*df*,2*p*) single-point energy calculations on MP2/6-31G(*d*) optimized geometries with scaled HF/6-31G(*d*) zero-point vibrational energies (ZPVE) and a so-called higher level correction (HLC). We have used a modified version of G2, namely G2(ZPE = MP2) [12], which employs scaled MP2/6-31G(*d*) frequencies rather that HF/6-31G(*d*), because of some small differences between the HF/6-31G(*d*) and MP2/6-31G(*d*) potential surfaces. We will refer to G2(ZPE = MP2) simply as G2 for the sake of brevity. The MP2 calculations are performed with correlation of all electrons, i.e. MP2(full).

Heats of formation at 298 K have been calculated using the atomization method, with temperature corrections applied as described by Nicolaides et al. [13] using an optimum low frequency scale factor of 1.0084 [14].

The energy dependence of the unimolecular rate constant $k(E)$ of a species has been calculated using RRKM theory [15], which can be formulated as

$$k(E) = \frac{\sigma N^{\ddagger}(E - E_0)}{h\rho(E)} \quad (1)$$

where E is the internal energy (relative to the reactant), E_0 is the energy of the transition structure, σ is the reaction path degeneracy, $N^{\ddagger}(E - E_0)$ is the number of states in the transition structure with energy less than or equal to E, $\rho(E)$ is the density of states of the reactant, and h is Planck's constant. Both the sum and density of states were obtained via direct count of the vibrational states using the Beyer-Swinehart algorithm [16]. The calculations employed MP2/6-31G(d) frequencies scaled using the optimum frequency scale factor of 0.9427 [14]. For fragmentation reactions, where no formal transition structure exists, the transition structure for formation of the product complex has been substituted.

Selected bond lengths are displayed in Figs. 1 and 2 and schematic energy profiles for the $[C_3H_8N]^+$ and $[C_3H_7S]^+$ systems are displayed in Figs. 3 and 4, respectively. Unless otherwise noted, all relative energies refer to G2 values at 0 K and structural data refer to MP2/6-31G(d) optimized geometries.

3. Discussion

3.1. Structural and energetic features of the $[C_3H_8N]^+$ surface

The lowest energy conformer of the species $[CH_3CH_2NHCH_2]^+$ (**1**) is shown in Fig. 1. All energies in the following section are given relative to that of **1**, unless otherwise noted.

We find two possible transition structures for the rearrangement of $[CH_3CH_2NHCH_2]^+$ (**1**) to $[CH_3CHNHCH_3]^+$ (**2**), which lies 38 kJ mol^{-1} below **1**. The first, lower-energy structure (**TSa:1 → 2**) corresponds to a 1,3-hydrogen shift and has a relative energy of 234 kJ mol^{-1}. The second (**TSb:1 → 2**) involves concerted 1,4- and 1,2-hydrogen shifts and lies at 289 kJ mol^{-1}.

Loss of molecular hydrogen from $[CH_3CHNHCH_3]^+$ (**2**) can occur via **TS:2 → 9**, which has an energy of 231 kJ mol^{-1}, leading to **9**. Ion **9** is a weak complex between molecular hydrogen and $[CH_2CHNHCH_2]^+$, which is bound by less than 1 kJ mol^{-1}. It dissociates to give these species, with a relative energy of 125 kJ mol^{-1}. We also find a transition structure (**TS:2 → 2′**) at 268 kJ mol^{-1} that will result in hydrogen exchange within the CH_3CH group of **2**, as discussed further below.

The $[CH_3CH_2NHCH_2]^+$ ion (**1**) can also rearrange to **3** via a 1,3-hydrogen shift (**TS:1 → 3**), with a barrier of 244 kJ mol^{-1}. Although we find no evidence for the existence of the previously proposed **1a** (Scheme 1) as a stable intermediate, **TS:1 → 3** does bear some resemblance to such a structure. The resulting ion **3** is best represented as the proton-bound complex $[CH_2CH_2 \cdots HNHCH_2]^+$. This complex contains very long C–H bonds (2.232 and 2.273 Å), which are significantly stretched compared with those in the isolated (bridged) ethyl cation [1.305 Å at MP2/6-31G(d)]. Ion **3** is stabilized by 40 kJ mol^{-1} with respect to its isolated components CH_2CH_2 and $[NH_2CH_2]^+$ and lies 87 kJ mol^{-1} above **1**.

Reorientation of the two components of the complex $[CH_2CH_2 \cdots HNHCH_2]^+$ (**3**) can occur via **TS:3 → 4**, with a relative energy of 105 kJ mol^{-1}, corresponding to a barrier from **3** of only 18 kJ mol^{-1}. The resulting ion–neutral complex **4**, which is best described as $[CH_2CH_2 \cdots CH_2NH_2]^+$, now has the ethylene carbons weakly bonded to the carbon atom from the $[NH_2CH_2]^+$ moiety, with long C–C bonds (2.891 Å). Ion **4** is stabilized by 25 kJ mol^{-1} with respect to CH_2CH_2 and $[NH_2CH_2]^+$ and lies 102 kJ mol^{-1} above **1**. Dissociation of either **3** or **4** results in ethylene plus $[CH_2NH_2]^+$ at 127 kJ mol^{-1}.

The complex **4** can undergo a concerted ring opening and 1,3-hydrogen shift to give $[CH_3CH_2CHNH_2]^+$ (**5**) at −25 kJ mol^{-1}. The transition structure (**TS:4 → 5**) for this process has an energy 191 kJ mol^{-1} above **1**.

Ion **5** can rearrange to $[CH_3CHCH_2NH_2]^+$ (**6**) via **TS:5 → 6** at a relative energy of 157 kJ mol^{-1}. The energy of **6** (164 kJ mol^{-1}), is actually higher than that of the transition structure for isomerization to **5** once zero-point vibrational energies are included, indicating that at best **6** lies in a shallow potential well. It is also possible for **4** to isomerize directly to **6** via **TS:4 → 6**, corresponding to a concerted ring opening and 1,2-hydrogen shift, with a relative energy of 222 kJ mol^{-1}.

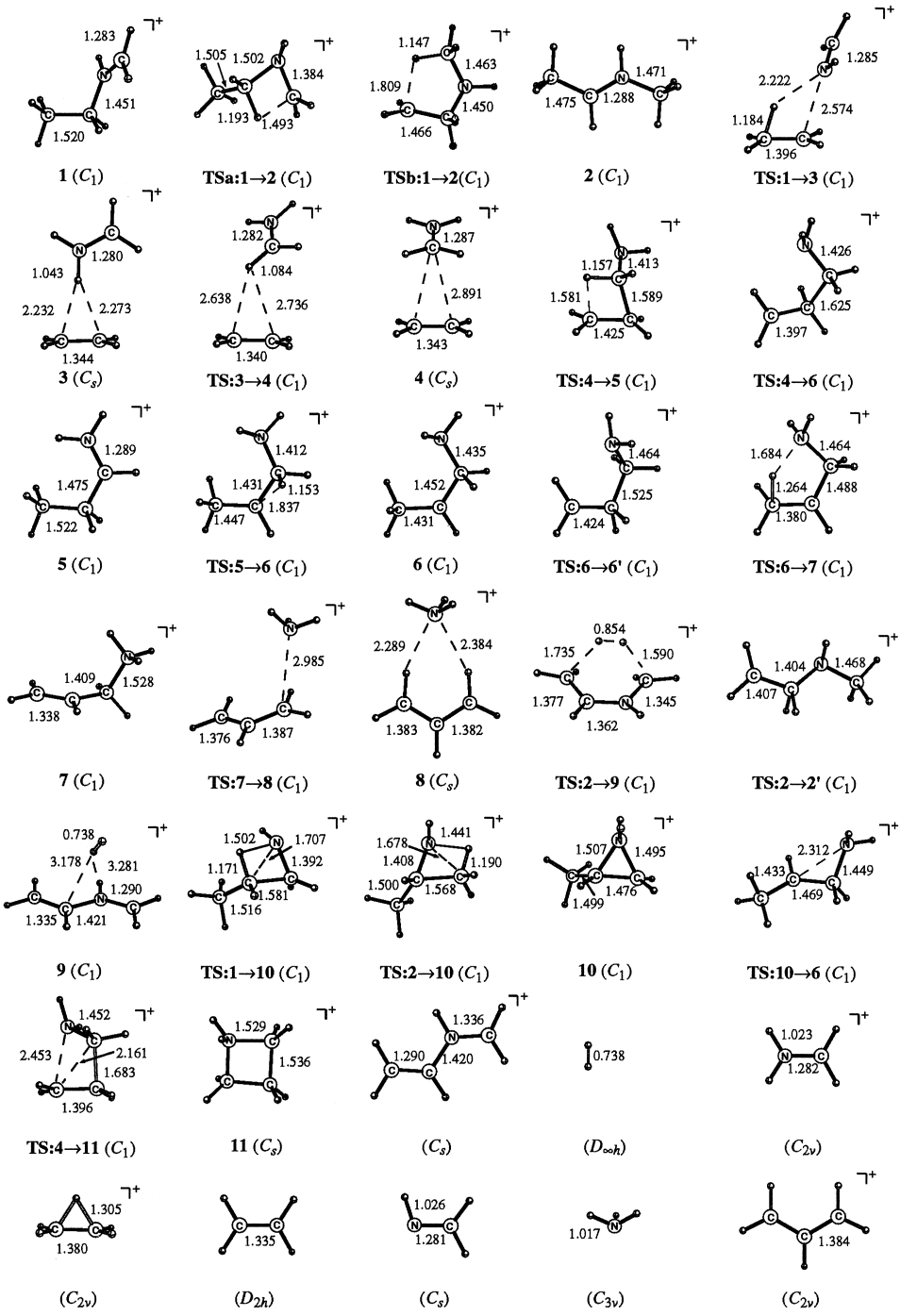

Fig. 1. Selected MP2/6-31G(d) bond lengths (Å) relevant to $[C_3H_8N]^+$ ions.

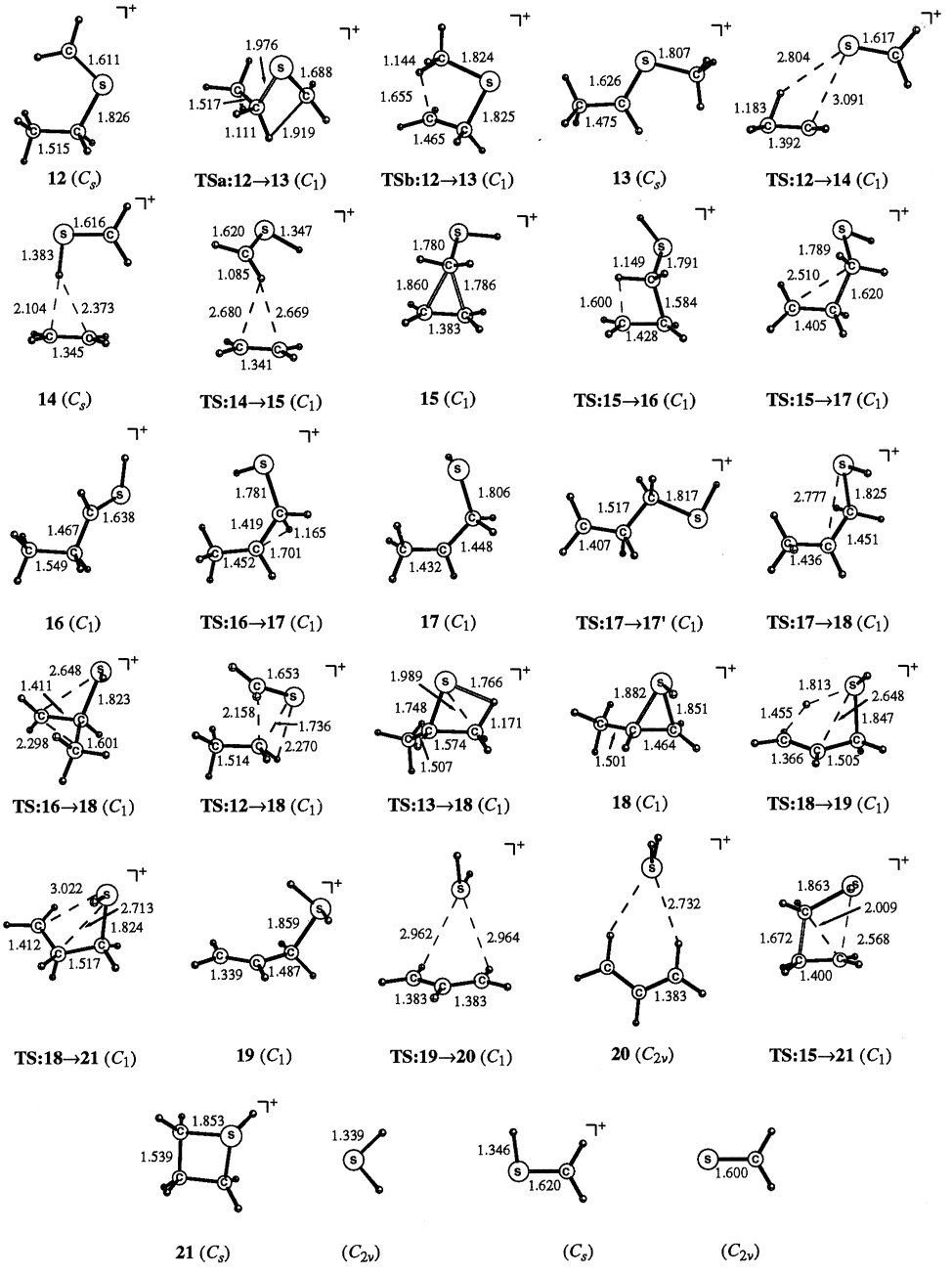

Fig. 2. Selected MP2/6-31G(*d*) bond lengths (Å) relevant to $[C_3H_7S]^+$ ions.

Another possible rearrangement of $[CH_2CH_2 \cdots CH_2NH_2]^+$ (**4**) leads to protonated azetidine (**11**) with a relative energy of 23 kJ mol^{-1}. The transition structure for this process (**TS:4** → **11**) lies at 226 kJ mol^{-1}. The role of **11** in labeling experiments will be discussed later.

More direct routes to the formation of $[CH_3CHCH_2NH_2]^+$ (**6**) from both **1** and **2** are also

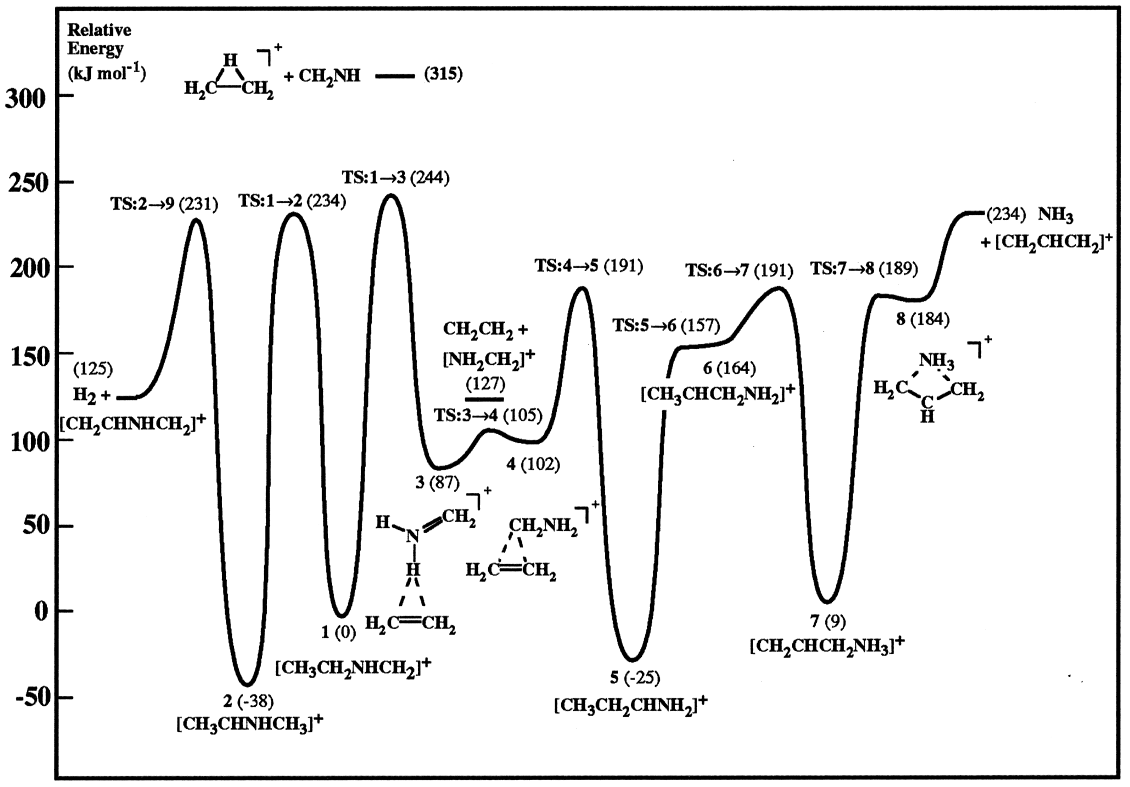

Fig. 3. Schematic energy profile for rearrangement/fragmentation of $[C_3H_8N]^+$ ions. Relative energies (kJ mol^{-1}) given in parentheses.

possible. Ions **1** and **2** can rearrange via 1,2-hydrogen shifts to form protonated methylaziridine (**10**) at 29 kJ mol^{-1}. Subsequent ring opening via **TS:10** → **6** at 176 kJ mol^{-1} results in the formation of **6**. However, the transition structures for these pathways have relative energies of 299 kJ mol^{-1} (**TS:1** → **10**) and 290 kJ mol^{-1} (**TS:2** → **10**) that are significantly higher than that required (244 kJ mol^{-1}) for formation of **6** from **1** and **2** via **4** and **5**, and will therefore most likely not be competitive.

Isomerization of $[CH_3CHCH_2NH_2]^+$ (**6**) to $[CH_2CHCH_2NH_3]^+$ (**7**) can occur via a 1,4-hydrogen shift (i.e. via **TS:6** → **7**) with an energy of 191 kJ mol^{-1}. Ion **7** is characterized by a long C–N bond (1.528 Å) and therefore already resembles in some respects a complex between the allyl cation and ammonia. However, the C–C bond lengths in **7** are still identifiable as single (1.409 Å) and double (1.338 Å), indicating a strongly distorted allyl cation. Although we find no evidence for the intermediate **6a** of Scheme 1, we do find a transition structure **TS:6** → **6′** at 236 kJ mol^{-1} that resembles **6a**. This transition structure results in exchange of hydrogens within the ethylidene (CH_3CH) group of **6**.

Migration of the ammonia moiety in $[CH_2CH\text{-}CH_2NH_3]^+$ (**7**) to a bridging position via **TS:7** → **8** at 189 kJ mol^{-1} gives **8**. Ion **8** can indeed be described as an ion–neutral complex between the allyl cation and ammonia. It lies 184 kJ mol^{-1} above **1** and is stabilized by 50 kJ mol^{-1} with respect to the separated species. Dissociation of the complex **8** or direct loss of ammonia from **7** results in the allyl cation plus ammonia, lying 234 kJ mol^{-1} above **1**.

The mechanism shown in Scheme 3 reflects the potential energy profile of Fig. 3. We find that the species **1a** and **6a** of Scheme 1 are actually transition

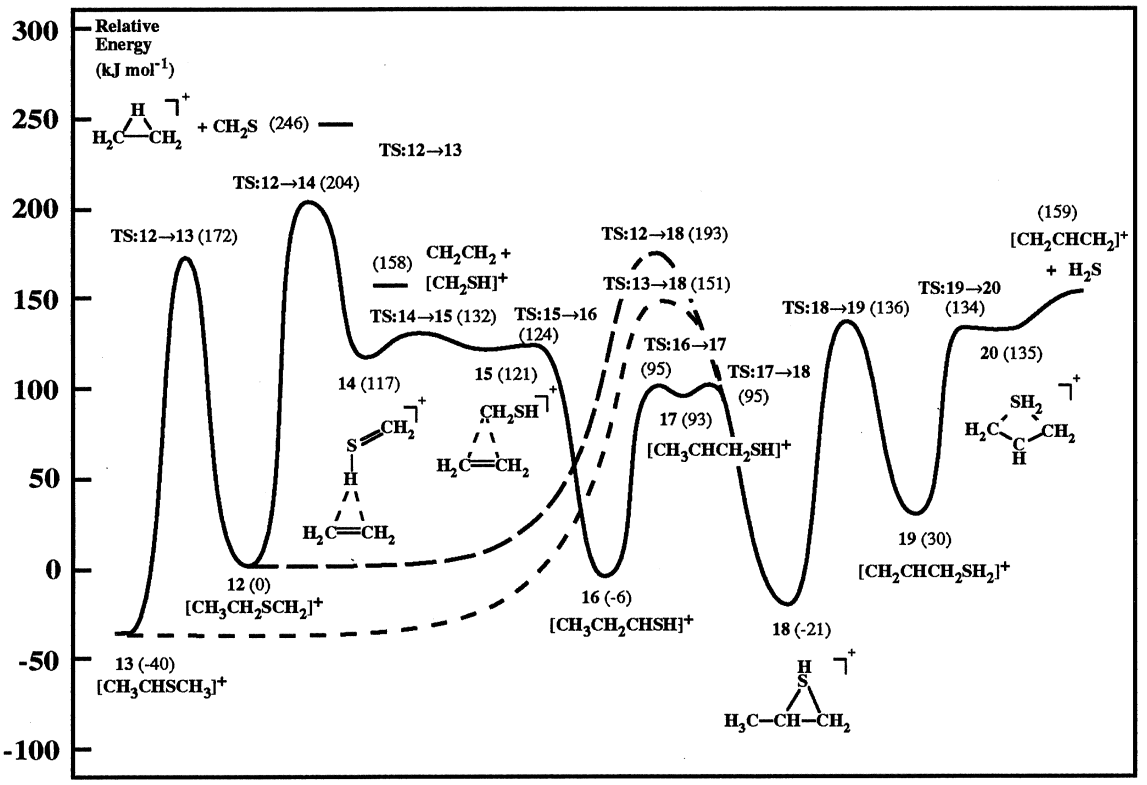

Fig. 4. Schematic energy profile for rearrangement/fragmentation of $[C_3H_7S]^+$ ions. Relative energies (kJ mol^{-1}) given in parentheses.

structures, with **6a** having a relatively high energy. Nevertheless, our calculations provide strong support for most aspects of the mechanism proposed by Bowen et al. [4c]. Our calculated surface is also found to be in good agreement with previous theoretical work [4a,6].

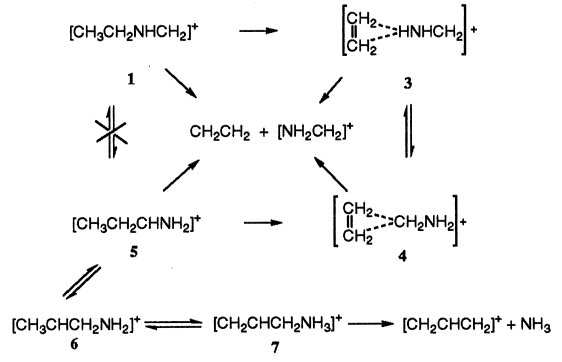

Scheme 3. Mechanism for rearrangement and fragmentation of $[C_3H_8N]^+$ ions based on the potential energy profile of Fig. 3

3.2. Structural and energetic features of the $[C_3H_7S]^+$ surface

The lowest energy conformer of $[CH_3CH_2SCH_2]^+$ (**12**) is shown in Fig. 2. All energies in the following section are given relative to that of **12**, unless otherwise stated.

We find two possible pathways for the isomerization of $[CH_3CH_2SCH_2]^+$ (**12**) to $[CH_3CHSCH_3]^+$ (**13**), which lies at −40 kJ mol^{-1} (Fig. 4). The first occurs via a 1,3-hydrogen shift (**TSa:12** → **13**) at 172 kJ mol^{-1} and the second occurs via concerted 1,4- and 1,2-hydrogen shifts (**TSb:12** → **13**) at 207 kJ mol^{-1}.

Alternatively, a 1,3-hydrogen shift in **12** can occur

via **TS:12** → **14** at 204 kJ mol^{-1}, resulting in **14**. This species is best described as an ion–neutral complex $[CH_2CH_2 \cdots HSCH_2]^+$, where the ethylene is bridged by a proton, with long C–H bonds (2.104 and 2.373 Å). Ion **14** has a relative energy of 117 kJ mol^{-1} and is stabilized by 41 kJ mol^{-1} with respect to the isolated species.

Reorientation within the complex $[CH_2CH_2 \cdots HSCH_2]^+$ (**14**) can occur via **TS:14** → **15** to form **15**, which has an energy of 121 kJ mol^{-1}. Ion **15** is also an ion–neutral complex, but in this case is best described as $[CH_2CH_2 \cdots CH_2SH]^+$ where the ethylene is bridged by a carbon atom, with elongated C–C bonds of 1.860 and 1.786 Å. The C–S bond is also extended by 0.160 Å, indicating a strong interaction between the two components of this complex. Ion **15**, lying at 121 kJ mol^{-1}, is stabilized by 37 kJ mol^{-1} relative to the isolated species. Dissociation of either **14** or **15** results in ethylene plus $[CH_2SH]^+$, with a relative energy of 158 kJ mol^{-1}.

The $[CH_2CH_2 \cdots CH_2SH]^+$ complex (**15**) lies in a very shallow well with a barrier of only 3 kJ mol^{-1} for its rearrangement (via **TS:15** → **16**) to $[CH_3CH_2CHSH]^+$ (**16**) at −6 kJ mol^{-1}.

Ion **15** can also rearrange to form protonated thietane (**21**) via **TS:15** → **21** at 157 kJ mol^{-1}. Protonated thietane (**21**) lies at an energy of 1 kJ mol^{-1} and is important in ^{13}C-label exchange as discussed below.

We find two pathways for the rearrangement of $[CH_3CH_2CHSH]^+$ (**16**) to protonated methylthiirane (**18**), which has a relative energy of −21 kJ mol^{-1}. The first is a stepwise route involving an initial 1,2-hydrogen shift (via **TS:16** → **17** at 95 kJ mol^{-1}) to form $[CH_3CHCH_2SH]^+$ (**17**) at 93 kJ mol^{-1}. Ion **17** can also be formed directly from **15** via **TS:15** → **17** at 159 kJ mol^{-1}. Subsequent ring closure in **17** via **TS:17** → **18** at 95 kJ mol^{-1} results in **18**. The second pathway via **TS:16** → **18** involves a 1,2-methyl shift and is distinguished first by its higher energy (154 kJ mol^{-1}) and second by the fact that it will result in an exchange of ^{13}C labels. This is discussed further below.

The ion **17a** from Scheme 2 corresponds to the transition structure **TS:17** → **17′**, which contributes to hydrogen exchange within **17** and lies at an energy of 173 kJ mol^{-1}.

An alternative pathway for the formation of protonated methylthiirane (**18**) has previously been suggested starting from **13** and involving a 1,2-hydrogen shift from carbon to sulfur and ring closure [5]. We find that this reaction can indeed occur, via **TS:13** → **18**, with a relative energy of 151 kJ mol^{-1}. We also find a pathway whereby **12** can directly rearrange to **18** as previously suggested [5]. This also occurs via a 1,2-hydrogen shift (**TS:12** → **18**), having a relative energy of 193 kJ mol^{-1}. The energies of the rate-limiting steps to direct isomerization to **18** from either **12** (via **TS:12** → **18**) of 172 kJ mol^{-1} or **13** (via **TS:13** → **18**) of 151 kJ mol^{-1} are actually lower than that for the rate-limiting step (via **TS:12** → **14**) for the ion-neutral complex mechanism discussed above of 204 kJ mol^{-1}.

A 1,4-hydrogen shift in protonated methylthiirane (**18**) via **TS:18** → **19** at 136 kJ mol^{-1} results in protonated allyl thiol $[CH_2CHCH_2SH_2]^+$ (**19**) with an energy of 30 kJ mol^{-1}. As for the analogous $[C_3H_8N]^+$ ion, we observe a long C–S bond (1.859 Å), suggesting a structure with an ion–neutral-complex character. However, the C–C bonds in **19** are still recognizable as single (1.487 Å) and double (1.339 Å), indicating considerable distortion in the complex between H_2S and the allyl cation. Ion **18** can also isomerize via **TS:18** → **21** (152 kJ mol^{-1}) to form protonated thietane (**21**) which is important in ^{13}C-label exchange.

Migration of the H_2S moiety in **19** yields the H_2S–allyl cation complex (**20**) at 135 kJ mol^{-1} via the transition structure **TS:19** → **20** at 134 kJ mol^{-1}. Dissociation of **20** or direct H_2S loss from **19** leads to H_2S plus $[CH_2CHCH_2]^+$, with a relative energy of 159 kJ mol^{-1}.

The mechanism shown in Scheme 4 is representative of the potential energy profile shown in Fig. 4. The main difference that we observe between the previously proposed mechanism of Scheme 2 and that reflecting our calculations and shown in Scheme 4 is the fact that **16a** corresponds not to a minimum but to a relatively high energy transition structure. We find that the "direct" pathways shown in Schemes 2 and 4

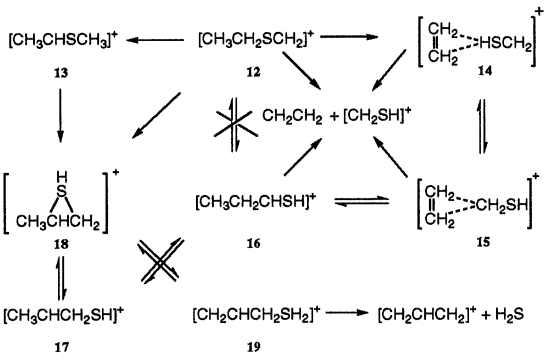

Scheme 4. Mechanism for rearrangement and fragmentation of $[C_3H_7S]^+$ ions based on the potential energy profile of Fig. 4

are actually lower in energy than the ion–neutral-complex–mediated mechanism (i.e. isomerization via **14** and **15**).

3.3. Comparisons with experimental thermochemical data

Calculated and experimental heats of formation ($\Delta_f H_{298}$) for $[C_3H_8N]^+$ ions and related species are presented in Table 1. Agreement between our calculated results and the experimental values from Lias et al. [17] is generally good but in some cases there are differences greater than 10 kJ mol^{-1}. Comparison with the rederived experimental values of Hammerum and Sølling [18] shows improved agreement, with all values but one being within the target error margin ($\pm$10 kJ mol^{-1}). For the CH_2NH plus $[CH_3CH_2]^+$ pair, the discrepancy is 48 kJ mol^{-1} but this is reduced to just 6 kJ mol^{-1} when a more recent value [19] for the heat of formation of CH_2NH is used.

Table 1
Calculated and experimental heats of formation for $[C_3H_8N]^+$ ions and related species (kJ mol^{-1})

Species		G2	Experiment[a]
$[CH_3CH_2NHCH_2]^+$	**1**	671	653, 666[b]
$[CH_3CHNHCH_3]^+$	**2**	632	615, 631[b]
$[CH_2CH_2 \ldots HNHCH_2]^+$	**3**	762	
$[CH_2CH_2 \ldots CH_2NH_2]^+$	**4**	776	
$[CH_3CH_2CHNH_2]^+$	**5**	644	636, 652[b]
$[CH_3CHCH_2NH_2]^+$	**6**	835	
$[CH_2CHCH_2NH_3]^+$	**7**	679	
$[CH_2CHCH_2 \ldots NH_3]^+$	**8**	860	
$[CH_2CHNHCH_2 \ldots H_2]^+$	**9**	804	
$[CH_2CH_2CH_2NH_2]^+$	**10**	690	698
$[CH_3CHCH_2NH_2]^+$	**11**	697	704
$NH_3 + [CH_2CHCH_2]^+$		910	900
$CH_2CH_2 + [NH_2CH_2]^+$		801	797, 804[b]
$CH_2NH + [CH_3CH_2]^+$		989	1037, 995[c]
$H_2 + [CH_2CHNHCH_2]^+$		802	

[a] All experimental values are taken from [17] unless otherwise noted.
[b] Values rederived in Hammerum and Sølling [18].
[c] Heat of formation for CH_2NH from [19].

Table 2
Calculated and experimental heats of formation for $[C_3H_7S]^+$ ions and related species (kJ mol^{-1})

Species		G2	Experiment[a]
$[CH_3CH_2SCH_2]^+$	**12**	770	803[b]
$[CH_3CHSCH_3]^+$	**13**	731	778[b]
$[CH_2CH_2 \ldots HSCH_2]^+$	**14**	892	
$[CH_2CH_2 \ldots CH_2SH]^+$	**15**	891	
$[CH_3CH_2CHSH]^+$	**16**	765	799[b]
$[CH_3CHCH_2SH]^+$	**17**	865	879[b]
$[CH_3CHCH_2SH]^+$	**18**	749	737, 774[b]
$[CH_2CHCH_2SH_2]^+$	**19**	801	
$[CH_2CHCH_2 \ldots SH_2]^+$	**20**	912	
$[CH_2CH_2CH_2SH]^+$	**21**	769	749, 799[b]
$H_2S + [CH_2CHCH_2]^+$		935	925, 920[b]
$CH_2CH_2 + [CH_2SH]^+$		933	914, 946[b]
$CH_2S + [CH_3CH_2]^+$		1020	1007

[a] All experimental values are taken from [17] unless otherwise noted.
[b] From Broer and Weringa [5a].

Heat of formation data relevant to the dissociation of $[C_3H_7S]^+$ ions and related species are listed in Table 2. The calculated values are consistently 10–20 kJ mol^{-1} greater than the values from Lias et al. [17]. The calculated heats of formation show even greater discrepancies when compared with experimental results from Broer and Weringa [5a], the differences being as large as 47 kJ mol^{-1}, suggesting that re-examination of the experimental data is desirable.

Comparisons with experimentally determined barrier heights can also be made. The barriers obtained [4c] from the appearance energies for ethylene loss from **1** and **5** of 293 and 296 kJ mol^{-1}, respectively, are significantly higher than the calculated values of 244 and 216 kJ mol^{-1}. However, since appearance energies provide an upper bound to the true barriers,

our results could be taken as being consistent with experiment. The barrier to ammonia loss from **7** is found experimentally to have a value of 255 kJ mol^{-1}, again somewhat higher than our calculated value of 225 kJ mol^{-1}.

Experimental barriers [5a] to ethylene loss from both **12** and **13** correspond to a relative energy of 222 kJ mol^{-1}, again higher than the calculated values of 172 and 158 kJ mol^{-1} for the rate-limiting steps from **12** and **13** (via **18**, respectively). Ethylene loss from **16** is found experimentally to have a barrier [5a] of 155 kJ mol^{-1}, quite close to the calculated value of 164 kJ mol^{-1}. It should be noted that these barriers were derived using the heats of formation from Broer and Weringa [5a] with which we have noted significant disagreement, and they would be altered by employing more accurate heats of formation for the relevant ions.

3.4. Rationalization of fragmentation behavior

There is extensive experimental information available concerning the fragmentation behavior of the $[C_3H_8N]^+$ and $[C_3H_7S]^+$ ions [4,5]. By examining the calculated potential energy surfaces and results of RRKM calculations, we attempt to rationalize the various observations.

3.4.1. $[CH_3CH_2NHCH_2]^+$ (1)

The only observed metastable elimination product from $[CH_3CH_2NHCH_2]^+$ (**1**) is ethylene [4]. This can be readily explained by examining the schematic energy profile shown in Fig. 3. A substantial barrier exists for isomerization of **1** to the ion–neutral complex **3**, and hence **3** will be formed with significant excess energy. In a situation such as this, dissociation will be favored over isomerization. Hence, fragmentation of the complex, leading to the elimination of ethylene, takes place before rearrangements that would result in the loss of other species can occur.

From the energy profile shown in Fig. 3 it would be reasonable to conclude that loss of molecular hydrogen from **1** could occur after isomerization to **2**. However, no such loss is observed experimentally [4f]. Comparison of the calculated log *k* versus *E* curves for the isomerization of **1** to **3** and for **2** going to **9** (Fig. 5) show that the latter is over two orders of magnitude smaller than the former in the internal energy range that is responsible for metastable dissociation (corresponding to rate constants between 10^4 and 10^6 s^{-1}). A full treatment of the kinetics of this two-well portion of the surface would result in a net rate constant for H_2 loss that is even smaller than k(**2** → **9**) due to the competitive back reaction from **2** to **1**. This is consistent with the absence of H_2 elimination from **1** that is observed experimentally.

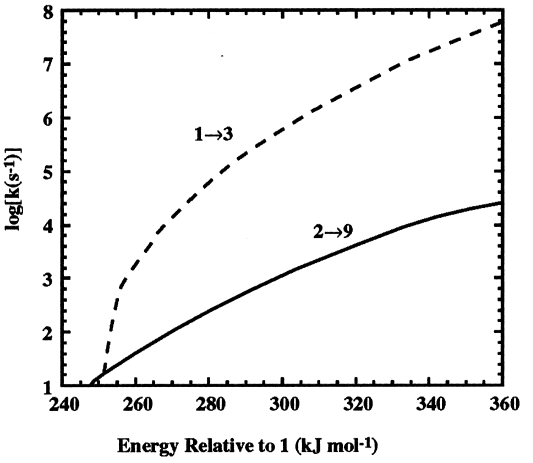

Fig. 5. RRKM rate constants (log *k*) calculated as a function of internal energy (*E*) for the dissociation of **1** to $C_2H_4 + NH_2CH_2^+$ (via isomerization to **3**) and dissociation of **2** to $H_2 + CH_2CHNHCH_2^+$ (via isomerization to **9**). Energy is measured relative to **1**.

3.4.2. $[CH_3CHNHCH_3]^+$ (2)

The metastable ion $[CH_3CHNHCH_3]^+$ (**2**) exhibits a competition between elimination of ethylene (~70%) and hydrogen (~30%) [4b,4f]. This is consistent with the surface discussed above for ion **1**. Even though k(**2** → **9**) is 100 times smaller that k(**1** → **3**), the backreaction from (**1** → **2**) will augment the net rate constant for H_2 elimination. This accounts for the dependence of the observations on whether the ion initially formed is **1** or **2**.

3.4.3. $[CH_3CH_2CHNH_2]^+$ (5)

Yet another distinct fragmentation pattern is shown by the metastable ion $[CH_3CH_2CHNH_2]^+$ (**5**), which

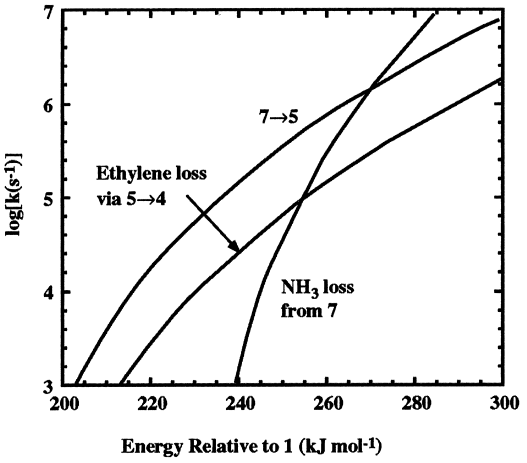

Fig. 6. RRKM rate constants (log k) calculated as a function of internal energy (E) for rearrangement/fragmentation processes from **5** and **7**. Energy is measured relative to **1**.

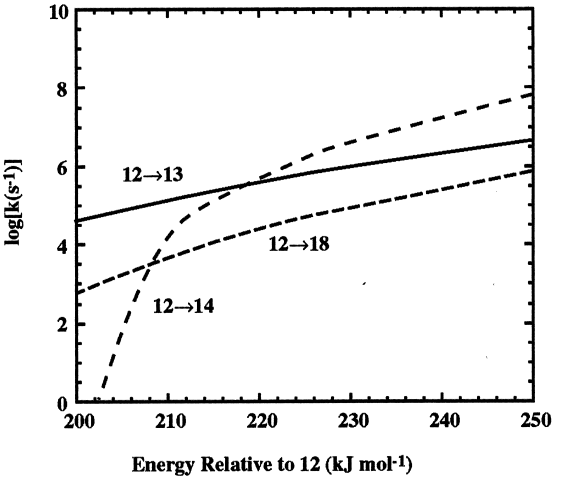

Fig. 7. RRKM rate constants (log k) calculated as a function of internal energy (E) for the rearrangement processes of **12**. Energy is measured relative to **12**.

eliminates both ethylene and ammonia, with the latter dominating [4]. It can be seen from Fig. 6 that the rates of ammonia elimination from **7** and ethylene loss from **5** (via **TS:4** $\rightarrow$ **5**) are similar in the rate constant region appropriate to metastable ions ($k = 10^4$–10^6 s^{-1}). However, the net rate constant for NH_3 loss from **5** will be reduced due to the competitive back-reaction of **7** to **5**. Thus, the calculated surface appears to be inconsistent with a dominance of NH_3 loss from **5**. This is addressed further in the light of isotopic labeling results (see Sec. 3.5.3).

3.4.4. $[CH_3CHSCH_3]^+$ (13) and $[CH_3CH_2CHSH]^+$ (16)

The metastable ions $[CH_3CHSCH_3]^+$ (**13**) and $[CH_3CH_2CHSH]^+$ (**16**) both eliminate roughly 38% ethylene and 62% hydrogen sulfide [5c]. However, different kinetic energy releases are observed, suggesting different rate-limiting steps for the elimination from the two ions. At first glance, it seems that this latter observation conflicts with our calculated surface (Fig. 4), which shows that **13** can rearrange to **18** below the threshold for ethylene elimination, thereby suggesting that the kinetic energy released during ethylene elimination should be the same for both these species. However, we find that isomerization of **13** to **18** does not occur with a sufficient rate to be experimentally significant ($\sim 10^4$ s^{-1}) until a relative energy of about 190 kJ mol^{-1} is reached. Thus, eliminations from the two ions have different rate-limiting steps and kinetic energy releases.

It remains to explain why **13** and **16** have similar fragmentation patterns [5c] despite the difference in their rate-limiting steps. The formation of ion **18** from **13** will result in **18** (or **16**) being produced with excess internal energy, which would normally be expected to affect the product distributions. However, since the dissociation limits and transition structure frequency factors for elimination of ethylene and hydrogen sulfide are similar, the branching ratio will not change greatly with internal energy.

3.4.5. $[CH_3CH_2SCH_2]^+$ (12)

The metastable ion $[CH_3CH_2SCH_2]^+$ (**12**) eliminates both ethylene (57%) and hydrogen sulfide (43%) [5c]. This surface is much more complicated than that for the nitrogen-containing ions because there are three competing isomerization reactions for this ion. By comparing the rate constants for these three channels, we may get an approximate indication of the product ratios. From Fig. 7 we see that when ion **12** is initially formed, there is roughly a 50–50 split between isomerization to **14** (and hence dissoci-

ation to form C_2H_4) and isomerization to **13**. Isomerization to **18** is a minor competitor. These results are consistent with the observation of competition between C_2H_4 and H_2S loss from this ion. To determine the exact branching ratios predicted from our surface, a full treatment of the kinetics would be necessary, which is outside the scope of the present study.

3.5. Labeling experiments

Numerous labeling studies have been carried out on both deuterated and ^{13}C-substituted isotopomers of the $[C_3H_7Z]^+$ ions. Our calculations can assist in the understanding of such experiments.

3.5.1. $[CH_3CH_2NHCH_2]^+$ (1)

Labeling experiments have shown that during ethylene elimination from $[CH_3CH_2NHCH_2]^+$ (**1**), β-hydrogen transfer to nitrogen occurs exclusively [4]. This is not surprising considering the mechanism discussed in Sec. 3.4.1. The initial isomerization step (via **TS:1** $\rightarrow$ **3**) involves transfer of a β-hydrogen to nitrogen (Fig. 1), and due to its high internal energy, the resulting complex will dissociate almost immediately. Hence, no further reactions that could result in label exchange occur.

3.5.2. $[CH_3CHNHCH_3]^+$ (2)

Based on labeling experiments for ethylene and hydrogen elimination from $[CH_3CHNHCH_3]^+$ (**2**), a mechanism suggesting complete exchange of the hydrogen atoms within the CH_3CH group has been proposed [4f]. The transition structure for this exchange (**TS:2** $\rightarrow$ **2′**) has an energy of 268 kJ mol^{-1}, which is somewhat higher than that for isomerization of either **2** to **3** or **2** to **9** (**TS:1** $\rightarrow$ **3** at 244 kJ mol^{-1} and **TS:2** $\rightarrow$ **9** at 231 kJ mol^{-1}, respectively).

Loss of molecular hydrogen from **2** involves abstraction of one hydrogen atom from each of the methyl groups (see **TS:2** $\rightarrow$ **9**, Fig. 1). If the exchange mechanism **2** $\rightarrow$ **2′** discussed previously is operating, it would be expected that the N-methyl group would contribute one hydrogen while the other hydrogen would come randomly from the CH_3CH group. Such a mechanism has previously been shown to agree well with the experimental results [4f].

3.5.3. $[CH_3CH_2CHNH_2]^+$ (5)

For the metastable ion $[CH_3CH_2CHNH_2]^+$ (**5**), labeling experiments suggest that in the first field-free region the nitrogen-bound hydrogens retain their identity but the remaining six hydrogens show complete exchange [4f]. For example, during ethylene loss from metastable $[CH_3CD_2CHNH_2]^+$ the observed abundances are 5% CH_2CH_2, 52% C_2H_3D, and 43% $C_2H_2D_2$ [4f] compared with the values of 7%, 54%, and 40%, respectively, expected for statistical exchange of all the alkyl hydrogens. Labeling experiments suggest a different behavior in the lower-energy second field-free region, with ethylene loss from $[CH_3CD_2CHNH_2]^+$ occurring in the proportions, 0% CH_2CH_2, 63% C_2H_3D, and 37% $C_2H_2D_2$ [4f]. This is close to the values of 0%, 67%, and 33%, respectively, predicted if exchange is restricted to the CX_2CX moiety.

The mechanism proposed to explain the observed label exchange in **5** involves sequential hydrogen shifts [4c,4d], and can be rationalized in terms of our calculated potential energy surface (Fig. 3). Reversible rearrangement of **5** and **6** results in exchange within the CH_2CH group. This occurs below the dissociation threshold and would therefore be expected to be rapid. In the lower-energy second field-free region, exchange is restricted to the CH_2CH group. Further exchange within **6**, occurring via **TS:6** $\rightarrow$ **6′**, which would result in a statistical distribution of carbon-bound hydrogens in **5**, would require a relative energy of 235 kJ mol^{-1}, or 44 kJ mol^{-1} more than that required for ethylene elimination. Although such exchange does not take place in the second field-free region, rearrangement via **TS:6** $\rightarrow$ **6′** becomes more favorable with the higher internal energies characteristic of the first field-free region, and exchange of all carbon-bound hydrogens is observed.

Now we must address the question of label retention of nitrogen-bound hydrogens in the loss of ethylene from **5**. We find that rearrangement of **7** to **5** is faster than ammonia loss from **7** (Fig. 6). This would seem to suggest that reversible isomerization of

7 and **5**, resulting in an exchange of nitrogen-bound and carbon-bound hydrogens, could occur. In previous theoretical work, a similar observation was made [4a], and was rationalized by suggesting that the calculated barrier for rearrangement of **7** to **5** was underestimated. Our confirmation of the relative barriers at a much higher level of theory would have seemed to make this explanation less likely but we note that, due to the steep nature of the log *k* versus *E* curve for ammonia loss from **7** (Fig. 6), only a modest increase in the energy of the transition structure for rearrangement of **7** to **5** (via **6**) relative to the energy of the isolated allyl cation and ammonia would be required to alter the ordering of the predicted relative rates. Ammonia loss from $[CH_3CH_2CHNH_2]^+$ (**5**) also displays a strong selectivity for retention of nitrogen-bound hydrogens. Again, this is consistent with an underestimation in the calculated barrier for the rearrangement of **5** to **7**, relative to that of fragmentation.

3.5.4. $[CH_3CH_2CHSH]^+$ (16)

On the basis of labeling studies on the metastable ion $[CH_3CH_2CHSH]^+$ (**16**), a mechanism involving incomplete exchange of the methyl hydrogens with the remaining alkyl hydrogens and only a small extent of exchange between sulfur-bound and alkyl hydrogens has been proposed [5b]. In contrast, our calculations suggest that the metastable ion **16** should undergo complete exchange of all alkyl hydrogens. Due to the low barriers to label-exchange processes such as isomerization of **16** to **17** and **16** to **15**, we would expect these processes to be rapid, resulting in a statistical distribution of labels on the alkyl chain. RRKM calculations support this conclusion, predicting that these processes should occur several orders of magnitude faster than dissociation.

We might expect that reversible isomerization of **19** to **18**, which also has a low barrier, would allow exchange between alkyl and sulfur-bound hydrogens. However, examination of the hydrogen sulfide loss from $[CH_3CH_2CHSH]^+$ (**16**) shows that again there is little exchange between the sulfur-bound and alkyl hydrogens [5b]. There is also incomplete exchange of the methyl hydrogens with the rest of the alkyl-chain, as indicated by the preference for the additional sulfur-bound hydrogen to originate from the methyl group.

3.5.5. $[CH_3CHSCH_3]^+$ (13)

A mechanism to explain the results of labeling experiments associated with the loss of ethylene from $[CH_3CHSCH_3]^+$ (**13**) has previously been suggested [5c]. This mechanism involves complete exchange of all but one hydrogen, the latter originating from the sulfur-bound methyl group. The isomerization of **13** to **18** involves a hydrogen shift from exactly this methyl group to sulfur.

3.5.6. $[CH_3CH_2SCH_2]^+$ (12)

As discussed in Sec. 3.4.5, ethylene elimination from $[CH_3CH_2SCH_2]^+$ (**12**) is predicted to occur to similar extents via rearrangement to **14** and to **13**. This would result in about 50% β-hydrogen transfer to sulfur from isomerization of **12** to **14** and 50% exhibiting the labeling behavior of ion **13**. Such a mechanism has previously been suggested and found to be in good agreement with experimental results [5b].

A mechanism for hydrogen sulfide loss from $[CH_3CH_2SCH_2]^+$ (**12**) that is consistent with experimental results has been proposed in which rearrangement of **12** to **18** and subsequent loss of H_2S can occur via two pathways [5b]. The first is rearrangement via **13** and **18**, as discussed for ethylene elimination above, and secondly, a direct route from **12** to **18**. While the log *k* versus *E* curves in Fig. 7 show that the first pathway is about an order of magnitude faster than direct isomerization of **12** to **18**, it is impossible to predict the real branching ratios without a complete analysis of the kinetics in terms of coupled rate equations.

3.5.7. ^{13}Carbon label studies

The study of ^{13}C-labeled species can give insight into the skeletal rearrangements that occur during the isomerization of metastable ions. No experimental ^{13}C-labeling results have been reported for the $[C_3H_8N]^+$ ions discussed here. However, on the basis of our calculated potential surface, we would expect

little ^{13}C-label exchange to occur in these systems. This type of exchange could potentially take place via reversible isomerization of protonated azeditine (**11**) and **4**. However, as discussed earlier, there are significant barriers to the formation of **4** from either $[CH_3CH_2NHCH_2]^+$ (**1**) or $[CH_3CH_2CHNH_2]^+$ (**5**), resulting in dissociation of the complex being faster than rearrangement processes, such as isomerization of **4** to **11**.

Experimental ^{13}C-labeling studies on $[C_3H_7S]^+$ ions have been performed and suggest that ^{13}C-label exchange occurs to a small extent [5b]. A mechanism to explain the results of these labeling studies suggested [5b] isomerization of $[CH_3CH_2CHSH]^+$ (**16**) to protonated methylthiirane (**18**) via the primary cation intermediate $[CH_3CH(SH)CH_2]^+$. This mechanism results in exchange of the α and β carbons within **16**. Although we find no evidence for an intermediate of this type, we do find a transition structure corresponding to it (**TS:16** $\rightarrow$ **18**). However, the energy requirement for this pathway is 59 kJ mol^{-1} higher than that for an alternative route via **TS:16** $\rightarrow$ **17** and **TS:17** $\rightarrow$ **18** that does not result in exchange of ^{13}C labels. Nevertheless, the energy required for rearrangement (via **TS:16** $\rightarrow$ **18**) is still below the dissociation limit so, although we would not expect there to be a large amount of ^{13}C-label exchange via this pathway, it is feasible that some exchange could occur.

It is also possible that ^{13}C-label exchange can occur via reversible isomerization of protonated methylthiirane (**18**) or the complex **15** with protonated thietane (**21**). The intervention of **TS:15** $\rightarrow$ **21** is distinguishable from the other possible mechanisms by virtue of the fact that it will result in exchange of all carbons. We cannot distinguish between these alternatives based on the available experimental data. Although the barriers to the isomerization processes via **21** of 157 and 152 kJ mol^{-1}, respectively, are just below the dissociation threshold, they must compete with many other low-energy processes, and therefore we would not expect a large extent of rearrangement to **21**. Hence, this route should also not lead to substantial ^{13}C-label exchange.

Table 3
Relative proton affinities (ΔPA)[a] of CH_2Z and CH_2CH_2, binding energies of $[CH_2CH_2 \cdots HZCH_2]^+$ complexes[b] and barriers for the rearrangement of $[CH_2CH_2 \cdots HZCH_2]^+$ to $[CH_3CH_2ZCH_2]^+$ (G2, kJ mol^{-1})

Z	ΔPA	Binding energy	Barrier
O	29	73	44
S	98	41	87
NH	185	40	157

[a] $\Delta PA = PA(CH_2Z) - PA(CH_2CH_2)$.
[b] Binding energy calculated with respect to CH_2CH_2 plus $[CH_2ZH]^+$.

3.6. When are ion–neutral complexes important?

We have noted several times in the present work that complexes that are formed with energy in excess of the dissociation limit are likely to fragment before they can be involved in any rearrangements. The principal origin of this excess energy is the presence of a reverse barrier for their formation. Hence, in order for ion–neutral complexes to be mechanistically significant intermediates, it is important that rearrangement to the complex occurs below the threshold for dissociation. We now examine some of the factors determining the relevant barriers for formation of $[CH_2CH_2 \cdots HZCH_2]^+$ complexes.

For both Z = S and NH, we find that the isomerization of $[CH_3CH_2ZCH_2]^+$ to the ion–neutral complex $[CH_2CH_2 \cdots HZCH_2]^+$ occurs above the dissociation limit, whereas for *Z* = O the isomerization was found to occur below the dissociation threshold [3]. Since $[CH_2CH_2 \cdots HZCH_2]^+$ is a proton-bound complex, it would be reasonable to suggest that its binding energy may in part be determined by the relative proton affinities of CH_2CH_2 and ZCH_2. It can be seen from Table 3 that there is indeed a correlation between the binding energy of the complex and the relative proton affinities (ΔPA). More closely matched proton affinities, i.e. lower values of ΔPA, allow greater sharing of the proton and hence a greater binding energy.

It can be seen from Table 3 that there is also a correlation between the relative proton affinities and the barriers for rearrangement of $[CH_2CH_2 \cdots HZCH_2]^+$ to $[CH_3CH_2ZCH_2]^+$. Lower values of ΔPA

are found to correspond to lower barriers. This result is not surprising when we examine the transition structures corresponding to this isomerization. It can be seen from Figs. 1 and 2 that transition structures **TS:1** $\rightarrow$ **3** and **TS:12** $\rightarrow$ **14** both resemble complexes between $[CH_3CH_2]^+$ and CH_2Z, as was previously found for Z = O [3]. A lower value of ΔPA results in the complex $[CH_3CH_2 \cdots ZCH_2]^+$, and therefore the barrier, being lower in energy relative to $[CH_2CH_2 \cdots HZCH_2]^+$. Hence, the barrier for rearrangement of $[CH_2CH_2 \cdots HZCH_2]^+$ to $[CH_3CH_2ZCH_2]^+$ will tend to be low if the species CH_2CH_2 and ZCH_2 have similar proton affinities.

The rearrangement of $[CH_2CH_2 \cdots CH_2NH_2]^+$ (**4**) to $[CH_3CH_2CHNH_2]^+$ (**5**) has a significant barrier (89 kJ mol^{-1}) and occurs above the threshold for ethylene elimination (Fig. 3). In contrast, the corresponding rearrangements of $[CH_2CH_2 \cdots CH_2OH]^+$ and $[CH_2CH_2 \cdots CH_2SH]^+$ (**15**) occur with much smaller barriers (18 and 3 kJ mol^{-1}, respectively) [3b], i.e. at energies below the dissociation limit.

We find that the barrier for rearrangement of the complex $[CH_2CH_2 \cdots CH_2ZH]^+$ to $[CH_3CH_2CHZH]^+$ can be related to the structure of the complex. The complex **15** (Fig. 2) has relatively short bridging C–C bonds (1.860 and 1.786 Å) and bears some resemblance to the transition structure **TS:15** $\rightarrow$ **16**. Consequently, the barrier is low (3 kJ mol^{-1}). In contrast, complex **4** has very long bridging C–C bonds (2.891 Å) and its structure is quite different from that of **TS:4** $\rightarrow$ **5**, resulting in a larger barrier (89 kJ mol^{-1}). Intermediate behavior in relation to both the structure of the complex (bridging C–C bond lengths of 1.932 and 1.946 Å) and barrier height (18 kJ mol^{-1}) was previously observed in the case of Z = O [3b]. This suggests that in situations of this type, the ion-neutral complex $[CH_2CH_2 \cdots CH_2ZH]^+$ can potentially play a more important role if it is tightly bound, i.e. if it has short bridging C–C bonds.

The lack of intervention by ion–neutral complexes can explain the observation that the ions $[CH_3CH_2NHCH_2]^+$ (**1**) and $[CH_3CH_2CHNH_2]^+$ (**5**) exhibit quite different behavior [4], as discussed earlier. In contrast, the ions $[CH_3CH_2CHOH]^+$ and $[CH_3CH_2OCH_2]^+$ can access these ion–neutral complexes and can therefore isomerize relatively easily, resulting in the observed similarity in fragmentation behavior for these two ions.

4. Concluding remarks

Ion–neutral complexes are found not to play an important role in the fragmentation/rearrangement mechanisms of the isomeric $[C_3H_8N]^+$ and $[C_3H_7S]^+$ ions. In the case of $[C_3H_8N]^+$ systems, this is a consequence of the presence of significant reverse barriers to the formation of the important ion–neutral complexes (**3** and **4**), with the result that the complexes undergo dissociation in preference to isomerization. For the $[C_3H_7S]^+$ systems, on the other hand, the ion–neutral complexes are not mechanistically important in determining the product abundances because there are lower-energy pathways via conventionally bonded intermediates. However, our results do suggest that the ion–neutral complex **15** could play a role in deuterium-label exchange. Apart from a few minor differences, the essential features of the mechanisms based on our potential energy surfaces (Schemes 3 and 4) are very similar to those previously proposed solely on the basis of experimental information (Schemes 1 and 2).

The calculated potential energy surfaces together with RRKM analyses lead to predictions that are consistent with most of the observed abundances of metastable ion dissociation products and with the results of labeling experiments. Our calculated heats of formation and barrier heights are also generally in satisfactory agreement with experiment, although in a few instances an experimental re-examination would be desirable.

Acknowledgements

The authors gratefully acknowledge generous allocations of time on the Fujitsu VPP300 and SGI Power Challenge computers of the Australian National University Supercomputing Facility.

References

[1] R.D. Bowen, D.H. Williams, J. Am Chem. Soc. 100 (1978) 7454.

[2] For recent reviews on ion–neutral complexes see, for example: (a) R.D. Bowen, Acc. Chem. Res. 24 (1991) 364; (b) P. Longevialle, Mass Spectrom. Rev. 11 (1992) 157; (c) D.J. McAdoo, T.H. Morton, Acc. Chem. Res. 26 (1993) 295.

[3] (a) G. Bouchoux, F. Penaud-Berruyer, H.E. Audier, P. Mourgues, J. Tortajada, J. Mass Spectrom. 32 (1997) 188; (b) A.J. Chalk, L. Radom, J. Am. Chem. Soc. 120 (1998) 8430.

[4] (a) G. Bouchoux, F. Penaud-Berruyer, J. Tortajada, Org. Mass Spectrom. 30 (1995) 723; (b) R.D. Bowen, Mass Spectrom. Rev. 96 (1991) 225; (c) R.D. Bowen, D.H. Williams, G. Hvistendahl, J.R. Kalman, Org. Mass Spectrom. 13 (1978) 721; (d) R.D. Bowen, D.H. Williams, J. Chem. Soc., Perkin Trans. 2 (1978) 1064; (e) K. Levson, F.W. McLafferty, J. Am. Chem. Soc. 96 (1974) 139; (f) N.A. Uccella, I. Howe, D.H. Williams, J. Chem. Soc. B (1971) 1933.

[5] (a) W.J. Broer, W.D. Weringa, Org. Mass Spectrom. 15 (1980) 229; (b) W.J. Broer, W.D. Weringa, ibid. 14 (1979) 36; (c) W.J. Broer, W.D. Weringa, ibid. 12 (1977) 326.

[6] C.E. Hudson, D.J. McAdoo, J. Am. Soc. Mass Spectrom. 9 (1998) 138.

[7] W.J. Hehre, L. Radom, P.v.R. Schleyer, J.A. Pople, Ab Initio Molecular Orbital Theory, Wiley, New York, 1986.

[8] M.J. Frisch, G.W. Trucks, H.B. Schlegel, P.M.W. Gill, B.G. Johnson, M.A. Robb, J.R. Cheeseman, T. Keith, G.A. Petersson, J.A. Montgomery, K. Raghavachari, M.A. Al-Laham, V.G. Zakrzewski, J.V. Ortiz, J.B. Foresman, J. Cioslowski, B.B. Stefanov, A. Nanayakkara, M. Challacombe, C.Y. Peng, P.Y. Ayala, W. Chen, M.W. Wong, J.L. Andres, E.S. Replogle, R. Gomperts, R.L. Martin, D.J. Fox, J.S. Binkley, D.J. DeFrees, J. Baker, J.J.P. Stewart, M. Head-Gordon, C. Gonzalez, J.A. Pople, GAUSSIAN 94 (rev. E.2), Gaussian, Inc., Pittsburgh, PA, 1995.

[9] MOLPRO96 is a package of ab initio programs written by H.J. Werner, P.J. Knowles with contributions from J. Almlof, R.D. Amos, M.J.O. Deegan, S.T. Elbert, C. Hampel, W. Meyer, K. Peterson, R. Pitzer, A.J. Stone, P.R. Taylor, R. Lindh, 1996.

[10] L.A. Curtiss, K. Raghavachari, G.W. Trucks, J.A. Pople, J. Chem. Phys. 94 (1991) 7221.

[11] For recent reviews on G2 theory, see: (a) L.A. Curtiss, K. Raghavachari, in Quantum Mechanical Electronic Structure Calculations with Chemical Accuracy, S.R. Langhoff (Ed.), Kluwer, Dordrecht, The Netherlands, 1995; (b) K. Raghavachari, L.A. Curtiss, in Modern Electronic Structure Theory, D.R. Yarkony (Ed.), World Scientific, Singapore, 1995.

[12] L.A. Curtiss, K. Raghavachari, J.A. Pople, J. Chem. Phys. 103 (1995) 4192.

[13] A. Nicolaides, A. Rauk, M.N. Glukhovtsev, L. Radom, J. Phys. Chem. 100 (1996) 17460.

[14] A.P. Scott, L. Radom, J. Phys. Chem. 100 (1996) 16502. The factor of 0.9427 is an optimum scale factor obtained by a least-squares procedure whereas the factor of 1.0084 is optimum for low frequencies.

[15] For a discussion of RRKM theory, see, (a) R.G. Gilbert, S.C. Smith, Theory of Unimolecular and Recombination Reactions, Blackwell Scientific, Oxford, 1990; (b) T. Baer, W.L. Hase, Unimolecular Reaction Dynamics Theory and Experiment, Oxford University Press, New York, 1996; (c) T. Baer, P.M. Mayer, J. Am. Soc. Mass Spectrom. 8 (1997) 103.

[16] T. Beyer, D.F. Swinehart, Comm. Assoc. Comput. Machines 16 (1973) 379.

[17] S.G. Lias, J.E. Bartmess, J.F. Liebman, J.L. Holmes, R.D. Levin, W.G. Mallard, J. Phys. Chem. Ref. Data Suppl. 17 (1988).

[18] S. Hammerum, T.I. Sølling, J. Am. Chem. Soc. 121 (1999) 6002.

[19] J.L. Holmes, F.P. Lossing, P.M. Mayer, Chem. Phys. Lett. 198 (1992) 285.